Title	Impact of soil erosion potential uncertainties on numerical simulations of the environmental fate of radiocesium in the Abukuma River basin
Author(s)	Ikenoue Tsubasa, Shimadera Hikari, Kondo Akira
Citation	Journal of Environmental Radioactivity, 225, p.106452_1-106452_12
Text Version	Accepted Manuscript
URL	https://jopss.jaea.go.jp/search/servlet/search?5068864
DOI	https://doi.org/10.1016/j.jenvrad.2020.106452
Right	©2020. This manuscript version is made available under the CC-BY-NC-ND4.0license http://creativecommons.org/licenses/by-nc-nd/4.0/. This is the accepted manuscript version. The formal published version is available at https://doi.org/10.1016/j.jenvrad.2020.106452

Impact of soil erosion potential uncertainties on numerical simulations of the environmental fate of radiocesium in the Abukuma River Basin

Tsubasa Ikenoue[a,*], Hikari Shimadera[b], Akira Kondo[b]

[a]Japan Atomic Energy Agency, 2-4 Shirakata, Tokai-mura, Naka-gun, Ibaraki 319-1195, Japan

[b]Osaka University, 2-1 Yamadaoka, Suita, Osaka 565-0871, Japan

[*] Corresponding author. E-mail address: ikenoue.tsubasa@jaea.go.jp

ABSTRACT

The Fukushima Dai-ichi Nuclear Power Plant accident in March 2011 resulted in the deposition of significant quantities of radionuclides, including radiocesium (^{137}Cs), over a wide area. Most of the deposited ^{137}Cs is strongly adsorbed on fine soil particles such as clay and silt near the ground surface. Therefore, to estimate the environmental fate of ^{137}Cs, it is necessary to predict its transport with eroded sediment in rainfall-runoff processes. In this study, a distributed radiocesium prediction model was applied to simulations of ^{137}Cs transport associated with hydrological processes in the Abukuma River Basin, the largest river system in Fukushima, over the period of 2011–2012. The soil erosion potential, which is a key input to the distributed radiocesium prediction model, was estimated using the Universal Soil Loss Equation (USLE). This study focused on the uncertainty in estimating the environmental fate of ^{137}Cs associated with the USLE factors. The USLE has five physically meaningful factors: the rainfall and runoff factor (R), soil erodibility factor (K), topographic factor (LS), cover and management factor (C), and support practice factor (P). Because the USLE factors were determined using various methods, R, LS, and the product of C and P ($C \times P$) were divided into two, three, and five cases, respectively, based on previous studies. Therefore, we conducted 30 different simulations. The average total ^{137}Cs outflow during the computational period in the simulation cases using the same USLE factors was 13.3 and 11.7 TBq for R (two cases), 12.6, 13.9 and 10.9 TBq for LS (three cases), and 26.5, 8.64, 0.47, 22.8 and 4.03 TBq for $C \times P$ (five cases). For the total outflow, C and P had the highest uncertainty of all the USLE factors. The outflow rates of the average total ^{137}Cs in the simulation cases using the same C and P from the croplands and forest areas and from the undisturbed

croplands and paddy fields were 62–91% and 18–34%, respectively. These results were due to the high erodibility of the croplands, the large forest areas in grids with high ^{137}Cs deposition density, and the high concentration of ^{137}Cs in the soil of the undisturbed croplands and paddy fields. This study indicates that land use, especially forest areas, croplands, and undisturbed paddy fields, has a significant impact on the environmental fate of ^{137}Cs.

Impact of soil erosion potential uncertainties on numerical simulations of the environmental fate of radiocesium in the Abukuma River Basin

1. Introduction

The Great East Japan Earthquake and its associated tsunami occurred on March 11, 2011, in Japan. The subsequent nuclear accident at the Fukushima Dai-ichi Nuclear Power Plant (FDNPP) resulted in the release of significant quantities of radionuclides into the atmosphere. These radionuclides were transported by atmospheric flows and deposited on the land surface via wet and dry deposition over a wide area around the FDNPP according to airborne monitoring by the Ministry of Education, Culture, Sports, Science and Technology (MEXT) et al. (2011a). MEXT and the Ministry of Agriculture, Forestry and Fisheries (MAFF) (2012) reported that the effective dose of radiocesium (^{134}Cs and ^{137}Cs) was much higher than that of other radionuclides at points where maximum amounts of radionuclides were detected. Although ^{134}Cs contributed to radiation dose of June 14, 2011 in the similar level of ^{137}Cs (MEXT and MAFF, 2012), half-life of ^{134}Cs is relatively shorter than that of ^{137}Cs. Therefore, to evaluate future radiation exposure doses, it is necessary to study ^{137}Cs.

In undisturbed soils, most of the deposited ^{137}Cs is distributed near the land surface and the concentration of ^{137}Cs decreases exponentially from the land surface with depth (Koarashi et al., 2012). In the topsoil, ^{137}Cs is localized in fine soil particles such as clay and silt (Sakaguchi et al., 2015). In the period from August 10, 2011, to May 11, 2012, it was estimated based on observations that 84–92% of the total ^{137}Cs transported in the Abukuma River Basin was carried in particulate form (Yamashiki et al., 2014). Considering these results, the soil erosion of the topsoil and subsequent sediment transport into the aquatic system, e.g., via rivers, is the primary mechanism for the migration of ^{137}Cs. Consequently, the long-term distribution of the air dose rate due to ^{137}Cs may be affected by rainfall-runoff processes. To

evaluate the environmental fate of ^{137}Cs and the future health effects of ^{137}Cs, it is necessary to predict sediment transport in rainfall-runoff processes.

Since the FDNPP accident, several numerical studies on the environmental fate of ^{137}Cs have been performed. Kurikami et al. (2014) applied one-dimensional sediment-contaminant transport code, Time-dependent, One-dimensional, Degradation And Migration (TODAM) (Onishi et al. 2007) to simulate the transport of ^{137}Cs in the Ogaki Dam Reservoir. They clarified the reservoir played an important role to delay and buffer the movement of ^{137}Cs in heavy rainfall events. Pratama et al. (2015) calculated the transport of ^{137}Cs adsorbed on soil particles in the Abukuma River Basin using a multiple compartment model. They predicted that the cumulative amount of ^{137}Cs discharged from the basin into the Pacific Ocean 100 years after the FDNPP accident would be 111 TBq. Kitamura et al. (2014) analyzed the transport of ^{137}Cs adsorbed on soil particles in 14 river basins including the Abukuma River Basin based on the Universal Soil Loss Equation (USLE) (Wischmeier and Smith, 1978) and simple sediment discharge formulas. They found an estimated annual amount of ^{137}Cs discharge to the ocean from the 14 river basins during 2011 of 8.4 TBq. Kinouchi et al. (2015) predicted the future transport of ^{137}Cs adsorbed on soil particles in the Kuchibuto River catchment based on a physically based distributed hydrological and sediment erosion model. According to their simulation, the amount of ^{137}Cs remaining in the catchment will be reduced to 39% of the initial total within 30 years of the FDNPP accident. Iwasaki et al. (2015) analyzed the transport of ^{137}Cs adsorbed on soil particles in the Abukuma River using a two-dimensional model. In their study, the calculated total ^{137}Cs export to the coastal area was 3.3 TBq in the period of September 22–24, 2011, when Typhoon Roke caused heavy precipitation in the basin. Wei et al. (2017) predicted the future transport of ^{137}Cs in the Kuchibuto River catchment in the Abukuma River Basin considering the size distribution of the soil particles and the leaching of ^{137}Cs from the forest canopy. Their result indicated that

0.57 TBq of ^{137}Cs was exported from the catchment between June 2011 and December 2014.

As mentioned above, several simulations of the transport of ^{137}Cs adsorbed on soil particles have been performed. The simulation results, however, vary substantially according to the uncertainty of the input data and parameters. Yoshimura et al. (2015) monitored ^{137}Cs wash-off associated with soil erosion in areas with different land use using USLE plots in Kawamata Town, Fukushima Prefecture, Japan. The monitoring results indicated that estimations of the concentration and wash-off of ^{137}Cs related to land use and the vegetation cover are crucially important to future modeling of the migration of ^{137}Cs inputs into river systems. Yamaguchi et al. (2014) conducted sensitivity analyses on the transport of sediment and ^{137}Cs in the study region of Kitamura et al. (2014) by changing the critical shear stress, the rainfall and runoff factor (R), which is one of the USLE factors, and other parameters. Their results indicated that R has a high sensitivity to sediment discharge.

Therefore, soil erosion is an important process in the transport of ^{137}Cs, and rainfall and land use have a large effect on the transport of ^{137}Cs. The USLE for estimating the soil erosion potential has five physically meaningful factors, and each factor has been determined using various methods. In this study, we focused on the uncertainty of the USLE factors and evaluated their impacts on the environmental fate of ^{137}Cs as simulated by a distributed radiocesium prediction model in the Abukuma River Basin.

2. Model

2.1 Distributed radiocesium prediction model

A distributed radiocesium prediction model was used to simulate the environmental fate of ^{137}Cs in the Abukuma River Basin. The distributed radiocesium prediction model is composed of a hydrological model, a sediment transport model, and a ^{137}Cs transport model. The hydrological model simulates water flow in the rainfall-runoff processes based on

geographical and meteorological data. Then, the sediment transport model calculates the transport of eroded soil based on the simulated water flow, and the ^{137}Cs transport model analyzes the transport of ^{137}Cs adsorbed on the eroded soil particles.

2.2 Hydrological model

The hydrological model is based on the distributed hydrological model of Kojiri et al. (2008). The hydrological model represents water cycle processes such as snowmelt, snowfall, infiltration, surface runoff, subsurface flow, and groundwater flow. In the hydrological model, the basin is divided into computational grids with a horizontal resolution of 1 km × 1 km and the computational grids act as the river flow network. Each computational grid consists of river and land of four layers (A, B, C, and D from top to bottom). In layer A, the grid is divided into four land use categories (croplands, forest areas, urban lands, and paddy fields). The land use characteristics depend on the land use ratio in each area. Infiltration and evapotranspiration are estimated by calculating the surface energy budget taking into account snowmelt and snowfall. In croplands, forest areas, and urban lands, the surface runoff is calculated by applying the kinematic wave model (Kojiri et al., 2008) to layer A. In paddy fields, a tank model is applied. The subsurface flow and moisture transport to each soil layer are calculated by applying a linear storage model (Kojiri et al., 2008) to layers B, C, and D. The soil moisture can move up and down between all of the layers. The groundwater flow is simulated in layer D. The water level and discharge are calculated by applying the kinematic wave model to the rivers. The three large dams in the Abukuma River Basin (Fig. 1) are simulated according to a simplified operation rule (Shrestha and Kondo, 2015) in the hydrological model.

The river network is a combination of multiple one-dimensional channels. The one-dimensional channels repeat confluence, and eventually all the channels confluent the

main channel and reach the estuary. A channel confluence is a collection of grids where several channels merge. The channel confluence is modeled so that the mass balance of the upstream and the downstream is equal. Sediment and ^{137}Cs transport are calculated based on the flow conditions at the same grid of the hydrological model. This calculation of confluence was applied to water, sediment and ^{137}Cs.

2.3 Sediment transport model

The sediment transport model considers advection, diffusion, sedimentation, resuspension, and the lateral inflow load of sediment. The one-dimensional mass balance of the suspended sediment in the rivers is expressed by Eq. (1):

$$\frac{\partial}{\partial t}(A_r C_{ss}) + \frac{\partial}{\partial x}(A_r U C_{ss}) = \frac{\partial}{\partial x}\left(A_r D_{ss} \frac{\partial C_{ss}}{\partial x}\right) - w_f \frac{A_r C_{ss}}{H_r} + q_{ss} \frac{A_r}{R_r} + f_{ss}, \quad (1)$$

$$w_f = \sqrt{\frac{2}{3}\left(\frac{\rho_{ss}}{\rho_w} - 1\right) g d_{ss} + \frac{36\nu^2}{{d_{ss}}^2}} - \frac{6\nu}{d_{ss}} \quad (2)$$

$$q_{ss} = \begin{cases} n_{ss}\left(\frac{u^{*2}}{{u_c}^{*2}} - 1\right)^{m_{ss}} & \text{when } u^* \geq {u_c}^* \\ 0 & \text{when } u^* < {u_c}^* \end{cases}, \quad (3)$$

where A_r is the stream cross-sectional area (m^2), C_{ss} is the suspended sediment concentration (g m^{-3}), U is the cross-sectional flow velocity (m s^{-1}), D_{ss} is the diffusion coefficient (m^2 s^{-1}), w_f is the settling velocity of the suspended sediment (m s^{-1}), H_r is the depth of the water (m), q_{ss} is the resuspension quantity per unit area (g m^{-2} s^{-1}), R_r is the hydraulic radius (m), f_{ss} is the lateral inflow load of the sediment (g m^{-1} s^{-1}), ρ_{ss} is the density of the sediment (g m^{-3}), ρ_w is the density of water (g m^{-3}), g is the gravitational acceleration (m s^{-2}), d_{ss} is the diameter of the soil particles (m), ν is the kinematic viscosity coefficient of water (g m^{-1} s^{-1}), n_{ss} is the constant of resuspension rate (g m^{-2} s^{-1}),

m_{ss} is the parameter of resuspension (-), u^* is the shear velocity (m s^{-1}), and $u_c{}^*$ is the critical shear velocity (m s^{-1}). w_f was obtained by using the empirical formula proposed by Rubey (1933). $u_c{}^*$ was calculated according to the experimental formula Iwagaki et al. (1956). To consider the difference in the runoff characteristics due to the diameter of the particles, the mobile soil particles were divided into four categories: clay, silt, fine sand, and coarse sand.

The USLE used to calculate f_{ss} is represented by

$$A = R \times K \times LS \times C \times P, \quad (4)$$

where A is the soil erosion rate per unit area (t ha^{-1} 10 min^{-1}), R is the rainfall and runoff factor (MJ mm ha^{-1} h^{-1} 10 min^{-1}), K is the soil erodibility factor (t h MJ^{-1} mm^{-1}), LS is the topographic factor (-), C is the cover and management factor or land use factor (-), and P is the support practice factor (-). The lateral inflow load of the sediment is

$$f_{ss} = SDR \frac{AW_{cell}}{6}, \quad (5)$$

where SDR is the sediment delivery ratio (-) and W_{cell} is the width of the computational grid (m).

2.4 ^{137}Cs transport model

Cesium-137 transport is modeled under the assumption that ^{137}Cs migrates with the eroded soil and does not dissolve in the river water. In the ^{137}Cs transport model, the suspended ^{137}Cs concentration in the channel flow is calculated based on the one-dimensional mass balance equation represented by

$$\frac{\partial}{\partial t}(A_r C_{ss} R_{riv}) + \frac{\partial}{\partial x}(A_r U C_{ss} R_{riv}) = \frac{\partial}{\partial x}\left(A_r D_{ss} \frac{\partial (C_{ss} R_{riv})}{\partial x}\right) - w_f \frac{A_r C_{ss} R_{riv}}{H_r} + q_{ss} R_{sed} \frac{A_r}{R_r} +$$

$$f_{ss} R_{top}, \quad (6)$$

where R_{riv}, R_{sed}, and R_{top} are the concentrations of ^{137}Cs (Bq g^{-1}) in the suspended sediment, the riverbed sediment, and the topsoil, respectively. The one-dimensional mass balance equation using this advection-diffusion equation is also used in TODAM. Kurikami et al. (2014) applied TODAM to simulate the transport of particulate and dissolved ^{137}Cs in the Ogaki Dam Reservoir. We assume that the ^{137}Cs deposited on the land surface is adsorbed on inorganic soil particles and does not interact with the organic matter. Considering that the ^{137}Cs concentration in the undisturbed soil decreases exponentially from the land surface with depth, R_{top} was calculated according to Kinouchi et al. (2015) as follows:

$$R_{soil}(z_r) = \begin{cases} 0 & \text{when } z_r > z_0 \\ R_{top} \exp(-k_r z_r) & \text{when } z_r \le z_0 \end{cases}, \quad (7)$$

$$R_{top} = \frac{k_r B_c}{\rho_B [1 - \exp(-k_r z_0)]} \exp(-\lambda t), \quad (8)$$

where R_{soil} is the concentration of ^{137}Cs in the soil (Bq g^{-1}), z_r is the depth from the topsoil (m), k_r is a relaxation constant (m^{-1}), B_c is the amount of deposited ^{137}Cs per unit area in the topsoil (Bq m^{-2}), ρ_B is the bulk density of the topsoil (g m^{-3}), z_0 is the depth of the on-site measurements (m), and λ is the decay constant (s^{-1}). R_{top} was estimated based on the results of the second airborne survey conducted in May 2011 (MEXT et al., 2011b), which represents the spatial distribution of ^{137}Cs within the top 5 cm (z_0) of the surface soil (B_c) as

171 validated by on-site measurements. We defined the soil of abandoned cultivated croplands,
172 forest areas, urban lands, and abandoned cultivated and planting restricted paddy fields as
173 undisturbed soil. Considering that the ^{137}Cs concentration in the disturbed soil is constant
174 regardless of the depth from the land surface, R_{top} is calculated as follows:
175
176 $$R_{soil}(z_r) = \begin{cases} 0 & \text{when } z_r > z_d \\ \frac{B_c}{\rho_B z_d} \exp(-\lambda t) & \text{when } z_r \leq z_d \end{cases} \quad (9)$$
177
178 where z_d is the depth of the soil disturbance (m). We defined the soil of the cultivated
179 croplands and paddy fields as disturbed soil.
180
181 **3. Computational conditions**
182 **3.1 Computational domain and period**
183 We simulated the transport of water, sediment, and ^{137}Cs in the Abukuma River Basin
184 (basin area $\approx$ 5400 km^2) as shown in Fig. 1. The Abukuma River Basin is located 30–100
185 km west of the FDNPP and is the largest of the basins in the Fukushima Prefecture. The
186 distributed radiocesium prediction model was applied to the Abukuma River Basin for the
187 period between January 2011 and December 2012. The transport of ^{137}Cs was simulated
188 starting on May 26, 2011, which was the final measurement day of the second airborne survey
189 (MEXT et al., 2011b). Figure. 2 shows the spatial distribution of the estimated ^{137}Cs
190 deposition density in the topsoil on the initial day. The model performance was evaluated at
191 observatories of the Ministry of Land, Infrastructure, Transport and Tourism (MLIT) along
192 the main channel of the Abukuma River (Fig. 1): nine sites (Kosakuda, Miyota, Akutsu,
193 Motomiya, Nihonmatsu, Kuroiwa, Fukushima, Fushiguro, and Yahata from upstream to
194 downstream) for the river discharge and two sites (Akutsu and Fushiguro) for the suspended

195 solid (SS).

196

197 **3.2 Target soil particles**

198 To consider the differences in runoff characteristics due to the particle diameter, the mobile
199 soil particles were divided into four classes: clay (0.45–2 μm), silt (2–20 μm), fine sand (20–
200 250 μm), and coarse sand (250–2000 μm). Based on the measurement result for the
201 contaminated soil in the eastern region of the Fukushima Prefecture according to Saito et al.
202 (2014), the mass fractions of the mobile soil particles in the topsoil were assumed to be 11.2%,
203 18.0%, 51.4%, and 19.4% for the clay, silt, fine sand, and coarse sand, respectively. Similarly,
204 based on the measurements of contaminated soil by Saito et al. (2014), 27.5%, 33.9%, 35.6%,
205 and 3.0% of the ^{137}Cs in the topsoil was assumed to be adsorbed on the clay, silt, fine sand,
206 and coarse sand particles, respectively.

207

208 **3.3 Input data**

209 Table 1 summarizes the main input data for the model simulation. Geographical data, such
210 as land use and elevation (Fig. 3.), for the hydrological model were obtained from the
211 National Land Numerical Information (NLNI) of MLIT (2011a). The rates of land use in the
212 Abukuma River Basin were 11.7%, 64.7%, 8.7%, and 14.8% for croplands, forest areas, urban
213 lands, and paddy fields, respectively. Observation data at six meteorological observatories and
214 28 Automated Meteorological Data Acquisition System (AMeDAS) stations (Fig. 1) by the
215 Japan Meteorological Agency (JMA) (2011) were used as meteorological inputs for the
216 hydrological model. At each computational grid, precipitation and other meteorological
217 variables were derived from observed data at the neighboring meteorological observatory or
218 AMeDAS station and at the neighboring meteorological observatory, respectively. For the
219 USLE in the sediment transport model, the precipitation data provided by JMA (2011) and the

geographical data provided by MLIT (2011a) were used to calculate R and the other factors, respectively. The spatial distribution of the deposited ^{137}Cs density in the study area (Fig. 2) and the ^{137}Cs concentration in the suspended and riverbed sediment provided by MEXT et al. (2011b) and MEXT (2012), respectively, were used for the initial conditions of the ^{137}Cs transport model. The areas of the abandoned cultivated fields and planting restricted paddy fields were provided by MAFF (2010) and MAFF (2011), respectively. The ratios of the undisturbed to disturbed areas were 0.093 and 0.065 for the croplands and paddy fields, respectively.

3.4 USLE factors

In this study, the soil erosion rate per unit area (A) was calculated for every 10-min period. R indicates the number of rainfall erosion index units plus a factor for runoff from snowmelt or applied water where such runoff is significant. Since the effects of snow melt and irrigation are limited to the western part of Fukushima Prefecture, Yamaguchi et al. (2014) omitted the effects. Similarly, the effects were omitted in this study. In this study, R was derived using two different calculation methods based on every 10 min of precipitation from the AMeDAS stations.

$$R_{USLE} = 0.119 + 0.0873 I_e I_{30} \log 6I_e, \quad (10)$$

$$R_{RUSLE} = 0.29(1 - 0.72 \exp(-0.05 \times 6I_e)) I_e I_{30}, \quad (11)$$

where R_{USLE} is the rainfall and runoff factor according to the USLE method (MJ mm ha^{-1} h^{-1} 10 min^{-1}), R_{RUSLE} is the rainfall and runoff factor according to the Revised Universal Soil Loss Equation (RUSLE) (Renard et al., 1997) method (MJ mm ha^{-1} h^{-1} 10 min^{-1}), I_e is the rainfall intensity (mm 10 min^{-1}), and I_{30} is the maximum 30-min rainfall intensity (mm).

The soil erodibility factor (K) is the soil loss rate per erosion index unit for a specified soil as measured on a unit plot, which is defined as a 22.1-m length with a continuous uniform 9% slope in clean-tilled fallow. In this study, K was derived from existing empirical values (Imai and Ishiwatari, 2007) for each specific soil type based on an MLIT (2007) soil map.

The topographic factor (LS) is the expected ratio of soil loss per unit area from the field slope to that from a 22.1-m length of uniform 9% slope under otherwise identical conditions. In this study, LS was derived using three different calculation methods based on elevation and the degree of slope tertiary mesh data from NLNI. LS is calculated as follows:

$$LS_{USLE} = \left(\frac{l}{22.1}\right)^{m} (65.41\sin^2\theta + 4.56\sin\theta + 0.065), \quad (12)$$

$$LS_{RUSLE} = \begin{cases} \left(\frac{l}{22.1}\right)^{\frac{\beta}{1+\beta}} (16.8\sin\theta - 0.5) \text{ when } s \leq 9\% \\ \left(\frac{l}{22.1}\right)^{\frac{\beta}{1+\beta}} (10.8\sin\theta + 0.03) \text{ when } s > 9\% \end{cases}, \quad (13)$$

$$\beta = \frac{\sin\theta}{0.0896(3\sin^{0.08}\theta + 0.56)}, \quad (14)$$

$$LS_{STREAM} = 1.4\left(\frac{A_s}{22.1}\right)^{0.04} \left(\frac{\sin\theta}{0.0896}\right)^{1.3}, \quad (15)$$

where LS_{USLE} is the topographic factor according to the USLE method (-), l is the slope length (m), θ is the angle of the slope (-), m is 0.5 if the slope gradient is 5% or more, 0.4 on slopes of 3.5–4.5%, 0.3 on slopes of 1–3%, and 0.2 on uniform gradients of less than 1%, β is the ratio of rill to interrill erosion, s is the slope gradient, LS_{RUSLE} is the topographic factor according to the RUSLE method (-), LS_{STREAM} is the topographic factor according to the stream power method (Moore et al., 1993) (-), and A_s is the area of the specific catchment or the upslope area per unit width of contour (m).

The cover and management factor (C) is the ratio of the soil loss from an area with a specified cover and management to that from an identical area in continuous tilled fallow. The

support practice factor (P) is the ratio of soil loss with a support practice such as contouring, strip cropping, or terracing to that with straight-row farming up and down the slope. In this study, C and P for each land use were derived from several different data sources based on land use tertiary mesh data from NLNI. The values of C and P were derived from two cases of C and P values according to the Japan Wildlife Research Center (JWRC) (2006) and Yamaguchi et al. (2013) from various Japanese sites. Yoshimura et al. (2015) monitored soil erosion under different land uses, and $C \times P$ was determined by calculating A, R, K, and LS based on the monitoring data. Similarly, we determined $C \times P$ based on soil erosion monitoring results in the Fukushima Prefecture (Japan Atomic Energy Agency, 2014; Niizato et al., 2016; Nishikiori et al., 2016; Wakabayashi et al., 2018; Wakiyama et al., 2019). $C \times P$ was derived for the three cases of minimum, maximum, and geometric mean based on the determined $C \times P$ values. Table 2 summarizes the $C \times P$ values used for the simulations.

As mentioned in the introduction section, we focused on the impact of the uncertainty of the USLE factors on the simulation of the environmental fate of ^{137}Cs. Because the USLE factors were determined using various methods, we conducted several simulations with various factors used in previous studies and compared the results to evaluate the effect of the uncertainty of the factors on the estimation of the ^{137}Cs transport. R and LS were divided into two and three cases, respectively, based on the differences in their calculation methods. $C \times P$ was divided into five cases according to the differences in the two organized data sources at the various Japanese sites and the soil erosion observation results in the Fukushima Prefecture. Accordingly, the soil erosion rate per unit area (A) was calculated for 30 different cases (Table 3).

Figure. 4 shows the distribution of the USLE factors in the computational domain. The total R during the computational period derived using the two methods had similar distributions and were high in the southwest and northwest regions of the Abukuma River Basin, where

293 there are large amounts of precipitation. K was high in the plain area, which had soil with
294 high erodibility, such as brown lowland soil. The LS values derived using the USLE and
295 RUSLE methods had similar distributions. Even though the LS values derived using the
296 stream power method were smaller than those derived using the other two methods, the LS
297 distributions derived from all three methods were high in the western region of the Abukuma
298 River Basin, where there are higher elevations. Even though some $C \times P$ values derived
299 from the various methods had different orders of magnitude, the $C \times P$ values in all cases
300 showed similar trends and were high in the croplands. However, the $C \times P$ values in the
301 minimum case were high not only in the croplands but also in the paddy fields; the $C \times P$
302 values in the paddy fields were higher than those in the croplands in only the minimum case.
303
304 **4. Results and discussion**
305 **4.1 River discharge and concentration of suspended sediments**
306 The hydrological model performance for simulating the daily river discharge was evaluated
307 using the statistical indices shown in Eqs. (16)–(18):
308
309 $$\mathrm{MBE} = \bar{M} - \bar{O}, \quad (16)$$
310 $$\mathrm{RMSE} = \left\{\frac{1}{N}\sum_{i=1}^{N}(M_i - O_i)^2\right\}^{\frac{1}{2}}, \quad (17)$$
311 $$\mathrm{NSE} = 1 - \frac{\sum_{i=1}^{N}(M_i - O_i)^2}{\sum_{i=1}^{N}(O_i - \bar{O})^2}, \quad (18)$$
312
313 where M is the calculated daily discharge ($m^3\ s^{-1}$), O is the observed daily discharge (m^3
314 s^{-1}), N is the number of samples (-), an overline indicates a sample mean, MBE is the mean
315 bias error ($m^3\ s^{-1}$), RMSE is the root mean square error ($m^3\ s^{-1}$), and NSE is the Nash–
316 Sutcliffe model efficiency coefficient (-). NSE, as defined by Nash and Sutcliffe (1970), is
317 often used to evaluate the reproducibility of discharge with a large fluctuation range; the

318 reproducibility of the model is good when the NSE value is 0.7 or more.

319 The statistical indices of the discharge during the computational period at each observatory
320 are shown in Table 4. The hydrological model performance was evaluated at nine sites along
321 the Abukuma River (Fig. 1) using the daily observation data of the river discharge provided
322 by MLIT (2011b). The number assigned to the discharge observatory in Fig. 1 increases from
323 upstream to downstream. In the calculation of MBE, RMSE, and NSE, the reproducibility of
324 the calculated discharge is good at all observatories.

325 The observed and calculated daily river flows at the Akutsu and Fushiguro observatories
326 are shown in Fig. 5. The calculated values at both observatories reproduced the trends of the
327 observed values at the times of flooding and normal flow, and the discharge increased from
328 upstream to downstream. When Typhoon Roke caused heavy precipitation in September 2011,
329 the calculated values at both observatories reached a maximum and reproduced the observed
330 values.

331 Figure. 6 shows the observed and calculated daily concentrations of suspended sediment at
332 the Akutsu and Fushiguro observatories. The concentrations were observed at the same points
333 as the discharge (MLIT, 2011b). In this study, we assumed the mass of the organic matter in
334 the SS was negligibly small so that the SS concentration could be regarded as that of the
335 suspended sediment. During normal flow, most of the observed values at both observatories
336 were within the range of the calculated values. During flooding, because there was no
337 observation data, we could not compare the calculated values to observations. According to
338 the model results, the concentration of suspended sediment rose even during short-term
339 precipitation events because R is proportional to the maximum 30-min rainfall intensity.

340

341 **4.2 Total suspended sediment and ^{137}Cs outflows**

342 The total suspended sediment and ^{137}Cs outflows during the computational period in the

343 Abukuma River Basin are shown in Fig. 7. The average total suspended sediment outflow
344 during the computational period in the simulation cases using the same USLE factors was
345 5.18 and 4.44 Tg for R (two cases), 4.84, 5.39 and 4.21 Tg for LS (three cases), and 7.99,
346 3.49, 0.10, 11.3 and 1.16 Tg for $C \times P$ (five cases). These average total outflows were listed
347 in ascending order of number indicating each USLE factors of the simulation case name. The
348 same is true for average total ^{137}Cs outflows described later. In the total suspended sediment
349 outflow, the ratio of the maximum (124_s) to minimum (233_s) values was 162. The average
350 total ^{137}Cs outflow during the computational period in the simulation cases using the same
351 USLE factors was 13.3 and 11.7 TBq for R, 12.6, 13.9 and 10.9 TBq for LS, and 26.5, 8.64,
352 0.47, 22.8 and 4.03 TBq for $C \times P$. In the total ^{137}Cs outflow, the ratio of the maximum
353 (121_s) to minimum (233_s) values was 87.2. The total suspended sediment outflow had a
354 higher uncertainty than the total ^{137}Cs outflow. In the total suspended sediment and ^{137}Cs
355 outflows, C and P had the highest uncertainty of all the USLE factors. These results
356 indicate that land use and support practice are important for the suspended sediment and ^{137}Cs
357 outflows. We achieved results similar to those of Yoshimura et al. (2015). Therefore, we
358 focused on the uncertainty of C and P.

359 Figure. 8 shows the outflow rates according to land use of the average total suspended
360 sediment and ^{137}Cs during the computational period in the simulation cases using the same
361 $C \times P$. In all the simulation cases, sum of the outflow rate of the average total ^{137}Cs from
362 croplands and forest areas was 62–91%. The $C \times P$ value of the croplands was large, and
363 grids with high ^{137}Cs deposition density had large forest areas. Therefore, the results indicate
364 that the ^{137}Cs outflow from forest areas and croplands was particularly important to the
365 dynamics of ^{137}Cs. The summed outflow rate of the average total ^{137}Cs from the undisturbed
366 croplands and paddy fields was 18–34%. Even if the ratio of undisturbed to disturbed areas
367 were less than 1%, this result would suggest that the impact on the ^{137}Cs outflow from

368 undisturbed croplands and paddy fields could not be ignored due to the high concentration of
369 ^{137}Cs in the surface undisturbed topsoil. The outflow rates of the average total suspended
370 sediment and ^{137}Cs from urban lands were small because $C \times P$ and the urban lands were
371 both small.

372 The Spatial distribution of the average total suspended sediment and ^{137}Cs outflow rates
373 during the computational period in the simulation cases using the same $C \times P$ are shown in
374 Figs. 9 and 10, respectively. The suspended sediment outflow rates in all cases show similar
375 trends and are large in the croplands. The ^{137}Cs outflow rates in all cases show similar trends
376 and are large in the croplands and in grids where the deposition density was high. The ratio of
377 the maximum to minimum values in the five $C \times P$ cases was nearly 1–3 at grids where the
378 suspended sediment and ^{137}Cs outflows were large. Therefore, the average total suspended
379 sediment and ^{137}Cs outflow rates at grids where the total outflow rate was large had very
380 similar distributions in all cases.

381

382 **4.3 Comparison of the calculated total exports to the total exports estimated in previous**
383 **studies**

384 Comparisons of the 30 each calculated total exports of suspended sediment and ^{137}Cs to the
385 values estimated based on previous studies are shown in Fig. 11. All of the estimated total
386 exports of suspended sediment and ^{137}Cs in Abukuma River basin based on observations and
387 other models were within the range of the calculated total exports. These results included
388 short-term flooding and long-term period total exports and the total exports in the Kuchibuto
389 River catchment where the deposition density was high. For the calculated total exports of
390 suspended sediment and ^{137}Cs during each the period of estimation, the ratios of the
391 maximum to minimum values were 46.5–94.1 and 41.7–53.2, respectively. The ratios of the
392 maximum to minimum values in the calculated total exports of suspended sediment and ^{137}Cs

during each the period of estimation were smaller than those in the calculated total suspended sediment and ^{137}Cs outflows. Most of the soil particles were transported in cases of small total export, even though most of the sand sunk and only clay and silt were transported in cases of large total export. Therefore, the calculated total exports of suspended sediment and ^{137}Cs had lower uncertainty than the calculated total exports.

5. Conclusions

In this study, we focused on the uncertainties of the USLE factors and evaluated their impacts on the environmental fate of ^{137}Cs as simulated by a distributed radiocesium prediction model in the Abukuma River Basin from January 2011 to December 2012. Because the USLE factors were determined using various methods, 30 simulations were performed with various factors used in previous studies. For the total suspended sediment and ^{137}Cs outflows during the computational period in the Abukuma River Basin, C and P had the highest uncertainty of all the USLE factors. Therefore, we focused on the uncertainty of C and P. The outflow rates of the average total ^{137}Cs in the simulation cases using the same $C \times P$ from croplands and forest areas was 62–91%. The outflow rates of the average total ^{137}Cs from the undisturbed croplands and paddy fields was 18–34% even when the ratio of the undisturbed to disturbed areas was less than 1%. The spatial distribution of the average total suspended sediment and ^{137}Cs outflow rates during the computational period in the simulation cases using the same $C \times P$ values showed similar trends. In the spatial distributions of all cases, the suspended sediment outflow rates were large in the croplands and the ^{137}Cs outflow rates were large in the croplands and in grids where the deposition density was high. These results were due to the high erodibility of the croplands, the large forest areas in grids with high ^{137}Cs deposition density, and the high concentration of ^{137}Cs in the soil of the undisturbed croplands and paddy fields. Therefore, land use, especially forest areas, croplands, and undisturbed

418 paddy fields, had a significant impact on the ^{137}Cs outflow.

419

420 References

421 • Imai, H., Ishiwatari, T., 2007. Regional characteristics of soil erosion factors in
422 prefectures based on such as statistical data, Monthly report, Civil Engineering Research
423 Institute for Cold Region No.645 (in Japanese).
424 https://thesis.ceri.go.jp/db/files/00160130701.pdf (accessed October 13, 2020)
425 • Iwagaki, Y., 1956. HYDRODYNAMICAL STUDY ON CRITICAL TRACTIVE FORCE.
426 Transactions of the Japan Society of Civil Engineers 41, 1-21. (in Japanese).
427 • Iwasaki, T., Nabi, M., Shimizu, Y., Kimura, I., 2015. Computational modeling of ^{137}Cs
428 contaminant transfer associated with sediment transport in Abukuma River. J. Environ.
429 Radioact. 139, 416-426. https://doi.org/10.1016/j.jenvrad.2014.05.012
430 • Japan Atomic Energy Agency (JAEA), 2014. Establishing assessment methods of a
431 long-term effect for radioactive matters associated with Fukushima Dai-ichi Nuclear
432 Power Plant accident in fiscal year 2013 (in Japanese).
433 https://radioactivity.nsr.go.jp/ja/list/504/list-1.html (accessed October 13, 2020)
434 • Japan Meteorological Agency (JMA), 2011. Climate Statistics (in Japanese).
435 http://www.jma.go.jp/jma/menu/report.html (accessed October 13, 2020)
436 • Japan Wildlife Research Center (JWRC), 2006. Information development survey report
437 by consignment of facilities development such as natural parks (in Japanese).
438 http://conservation.jp/tanzawa/online/nagare_03chousa/chousa/H17_12_itaku_johoseibic
439 hosa_1.pdf (accessed October 13, 2020)
440 • Kanda, J., 2012. Long-term sources: To what extent are marine sediments, coastal
441 groundwater, and rivers a source of ongoing contamination? In: Fukushima Ocean
442 Impacts Symposium: Exploring the Impacts of the Fukushima Dai-ichi Nuclear Power

443 Plant Accidents on the Ocean, November 13, Sanjo Conference Hall, University of Tokyo,
444 Japan. https://www.whoi.edu/website/fukushima-symposium/presentation-files (accessed
445 October 13, 2020)
446 • Kinouchi, T., Yoshimura, K., Omata, T., 2015. Modeling radiocesium transport from a
447 river catchment based on a physically-based distributed hydrological and sediment
448 erosion model J. Environ. Radioact. 139, 407-415.
449 https://doi.org/10.1016/j.jenvrad.2014.07.022
450 • Kitamura, A., Yamaguchi, M., Kurikami, H., Yui, M., Onishi, Y., 2014. Predicting
451 sediment and cesium-137 discharge from catchments in eastern Fukushima.
452 Anthropocene. 5, 22-31. https://doi.org/10.1016/j.ancene.2014.07.001
453 • Koarashi, J., Atarashi-Andoh, M., Matsunaga, T., Sato, T., Nagao, S., Nagai, H., 2012.
454 Factors affecting vertical distribution of Fukushima accident-derived radiocesium in soil
455 under different land-use conditions. Science of The Total Environment. 431, 392-401.
456 https://doi.org/10.1016/j.scitotenv.2012.05.041
457 • Kojiri, T., Hamaguchi, T., Ode, M., 2008. Assessment of global warming impacts on
458 water resources and ecology of a river basin in Japan. Journal of Hydro-environment
459 Research. 1, 164–175. https://doi.org/10.1016/j.jher.2008.01.002
460 • Kurikami, H., Kitamura, A., Yokuda, S.T. and Onishi, Y., 2014. Sediment and ^{137}Cs
461 behaviors in the Ogaki Dam Reservoir during a heavy rainfall event. J. Environ. Radioact.
462 137, 10–17. https://doi.org/10.1016/j.jenvrad.2014.06.013
463 • MAFF (Ministry of Agriculture, Forestry and Fisheries, Japan), 2010. Census of
464 agriculture and forestry.
465 • MAFF (Ministry of Agriculture, Forestry and Fisheries, Japan), 2011. Information of the
466 Great East Japan Earthquake (in Japanese).
467 http://www.maff.go.jp/j/kanbo/joho/saigai/s_seisan.html (accessed October 13, 2020)

- Ministry of Education, Culture, Sports, Science and Technology, Japan (MEXT), U.S. Department of Energy, Nuclear Regulation Authority, 2011a. Air Dose Rate Results of the First Airborne Monitoring Survey. https://emdb.jaea.go.jp/emdb/en/portals/b1010301/ (accessed October 13, 2020)
- Ministry of Education, Culture, Sports, Science and Technology, Japan (MEXT), U.S. Department of Energy, Nuclear Regulation Authority, 2011b. Results of Deposition of Radioactive Cesium of the Second Airborne Monitoring Survey. https://emdb.jaea.go.jp/emdb/en/portals/b1020201/ (accessed October 13, 2020)
- Ministry of Education, Culture, Sports, Science and Technology, Japan (MEXT), 2012. Report on radiation dose distribution map related research Part 2 (in Japanese). http://radioactivity.nsr.go.jp/ja/contents/6000/5522/25/5600_201203131000_report2-1.pdf (accessed October 13, 2020)
- Ministry of Education, Culture, Sports, Science and Technology, Japan (MEXT), Ministry of Agriculture, Forestry and Fisheries, Japan (MAFF), 2012. Summarized Version of the "Results of the Research on Distribution of Radioactive Substances Discharged by the Accident at TEPCO's Fukushima Dai-ichi NPP". http://radioactivity.nsr.go.jp/en/contents/1000/294/24/PressR04%200802s.pdf (accessed October 13, 2020)
- Ministry of Land, Infrastructure, Transport and Tourism, Japan (MLIT), 2007. Land Classification Survey (in Japanese). https://nlftp.mlit.go.jp/kokjo/inspect/inspect.html (accessed October 13, 2020)
- Ministry of Land, Infrastructure, Transport and Tourism, Japan (MILT), 2011a. National Land Numerical Information (NLNI) Download Service (in Japanese). https://nlftp.mlit.go.jp/ksj/ (accessed October 13, 2020)
- Ministry of Land, Infrastructure, Transport and Tourism, Japan (MLIT), 2011b. Water

493 Information System (in Japanese). http://www1.river.go.jp (accessed October 132020)
494 • Moore, I.D., Turner, A.K., Wilson, J.P., Jenson, S.K., Band, L.E. 1993. GIS and
495 Land-Surface-Subsurface Process Modeling, Enviromental Modeling with GIS, Oxford
496 university Press, 196-230.
497 • Nash J. E., Sutcliffe J. V., 1970. River flow forecasting through conceptual models part I
498 — A discussion of principles. Journal of Hydrology, 10, 282-290.
499 https://doi.org/10.1016/0022-1694(70)90255-6
500 • Niizato, T., Abe, H., Mitachi, K., Sasaki, Y., Ishi, Y., Watanabe., T., 2016. Input and
501 output budgets of radiocesium concerning the forest floor in the mountain forest of
502 Fukushima released from the TEPCO's Fukushima Dai-ichi nuclear power plant accident.
503 J. Environ. Radioact. 161, 11-21. http://dx.doi.org/10.1016/j.jenvrad.2016.04.017
504 • Nishikiori, T., Ito, S., Tsuji, H., Yasutaka, T., Hayashi, S., 2015. Influence of Forest Floor
505 Covering on Radiocesium Wash-off Associated with Forest Soil Erosion. Journal of the
506 Japanese Forest Society. 97, 63-69 (in Japanese). https://doi.org/10.4005/jjfs.97.63
507 • Onishi, Y., Voitsehkovich, Ov., Zheleznyak, MJ., 2007. Chernobyl – What Have We
508 learned? The Successes and Failures to Mitigate Water Contamination Over 20 years.
509 Springer Publishers, Dordrecht, The Netherlands.
510 • Pratama, M.A., Yoneda, M., Shimada Y., Matsui, Y., Yamashiki, Y., 2015. Future
511 projection of radiocesium flux to the ocean from the largest river impacted by Fukushima
512 Daiichi Nuclear Power Plant Scientific Reports. Sci. Rep.
513 http://dx.doi.org/10.1038/srep08408
514 • Renard, K.G., Foster, G.R., Weesies, G.A., McCool, D.K., Yoder, D.C., Coordinators.
515 1997. Predicting soil erosion by water: A guide to conservation planning with the Revised
516 Universal Soil Loss Equation (RUSLE). U.S. Department of Agriculture Agriculture
517 Handbook No. 703.

518 • Saito, T., Makino, H., Tanka, S., 2014. Geochemical and grain-size distribution of
519 radioactive and stable cesium in Fukushima soils: implications for their long-term
520 behavior. J. Environ. Radioact. 138, 11-18.
521 http://dx.doi.org/10.1016/j.jenvrad.2014.07.025
522 • Sakaguchi, A., Tanaka, K., Iwatani, H., Chiga, H., Fan, Q., Onda, Y., Takahashi, Y., 2015.
523 Size distribution studies of ^{137}Cs in river water in the Abukuma riverine system following
524 the Fukushima Dai-ichi Nuclear Power Plant accident. J. Environ. Radioact. 139,
525 379-389. https://doi.org/10.1016/j.jenvrad.2014.05.011
526 • Shrestha, K.L., Kondo, A., 2015. Assessment of the Water Resource of the Yodo River
527 Basin in Japan Using a Distributed Hydrological Model Coupled with WRF Model.
528 Environmental Management of River Basin Ecosystems. 137-160.
529 https://doi.org/10.1007/978-3-319-13425-3_8
530 • Wakabayashi, S., Eguchi, T., Ota, T., Matsunami, H., Yoshino, N., Higashiyama, M., 2018.
531 Effect of cover crops on cesium-137 runoff control in sloping fields. Japanese Journal of
532 Soil Science and Plant Nutrition. 89, 19-25 (in Japanese).
533 https://doi.org/10.20710/dojo.89.1_19
534 • Wakiyama, Y., Onda, Y., Yoshimura, K., Igarashi, Y., Kato, H., 2019. Land use types
535 control solid wash-off rate and entrainment coefficient of Fukushima-derived ^{137}Cs, and
536 their time dependence. J. Environ. Radioact. 210, 105990.
537 https://doi.org/10.1016/j.jenvrad.2019.105990
538 • Wei, L., Kinouchi, T.,Yoshimura, K., Velleux, M.L., 2017. Modeling watershed-scale
539 ^{137}Cs transport in a forested catchment affected by the Fukushima Dai-ichi Nuclear Power
540 Plant accident. J. Environ. Radioact. 171, 21-33.
541 https://doi.org/10.1016/j.jenvrad.2017.01.017
542 • Wischmeier, W.H., Smith, D.D., 1978. Predicting Rainfall Erosion Losses – A Guide to

543 Conservation Planning. U.S. Department of Agriculture Agriculture Handbook No. 537.
544 • Yamaguchi, M., Maekawa, K., Takeuchi, S., Kitamura, A., Onishi, Y., 2013. evelopment
545 of a model to predict a radionuclide distribution based on soil migration after Fukushima
546 Dai-ichi Nuclear Power Plant accident. Journal of Nuclear Fuel Cycle and Environment.
547 20, 53-70 (in Japanese). https://nuce.aesj.or.jp/jnuce/vol20/Jnuce-Vol20-2-p53-70.pdf
548 (accessed October 13, 2020)
549 • Yamaguchi M., Kitamura A., Oda Y., Onishi Y., 2014. Predicting the long-term ^{137}Cs
550 distribution in Fukushima after the Fukushima Dai-ichi nuclear power plant accident: a
551 parameter sensitivity analysis. J. Environ. Radioact. 135, 135-146.
552 https://doi.org/10.1016/j.jenvrad.2014.04.011
553 • Yamashiki, Y., Onda, Y., Smith, H.G., Blake, W.H., Wakahara, T., Igarashi, Y., Matsuura,
554 Y., Yoshimura, K., 2014. Initial flux of sediment-associated radiocesium to the ocean
555 from the largest river impacted by Fukushima Daiichi Nuclear Power Plant. Sci. Rep.
556 http://dx.doi.org/10.1038/srep03714
557 • Yoshimura, K., Onda, Y., Kato, H., 2015. Evaluation of radiocaesium wash-off by soil
558 erosion from various land uses using USLE plots. J. Environ. Radioact. 139, 362-369.
559 https://doi.org/10.1016/j.jenvrad.2014.07.019

Table 1.

List of the main input data used for the model simulation.

Model	Item	Source
Hydrological model	Elevation	1-km resolution data by MLIT (2011a)
	Land use	1-km resolution data by MLIT (2011a)
	Watershed boundary	100-m resolution data MLIT (2011a)
	Stream channel	MLIT (2011a)
	Dam	MLIT (2011a)
	Precipitation	Hourly data at meteorological observatories and AMeDAS stations by JMA (2011)
	Air tempreature, wind velocity, water vapor pressure, atmosphreic pressure, solar irradiance	Hourly data at meteorological observatories by JMA (2011)
Sediment transport model	Precipitation for R	10-minute data at meteorological observatories and AMeDAS stations by JMA (2011)
	Soil type for K	Land classification basic survey by MLIT (2007) (1:50000 scale map)
	Elevation for LS	250-m resolution data by MLIT (2011a)
	Land use for C and P	1-km resolution data by MLIT (2011a)
^{137}Cs transport model	Initial ^{137}Cs distribution in land	MEXT et al. (2011b)
	Initial ^{137}Cs concentration in riverbed	MEXT (2012)
	Area of abandoned cultivated filelds	MAFF (2010)
	Area of planting restricted paddy fields	MAFF (2011)

Table 2.

List of $C \times P$ values used in the simulations.

Data	Forest areas	Croplands	Paddy fields	Urban lands
Organized data source at various Japanese sites by Yamaguchi et al. (2013)	6.00×10^{-3}	2.64×10^{-1}	1.05×10^{-1}	1.00×10^{-2}
Organized data source at various Japanese sites by JWRC (2006)	1.00×10^{-3}	1.60×10^{-1}	3.00×10^{-2}	0.00
Minimum case based on the Fukushima monitoring data	9.37×10^{-5}	1.20×10^{-3}	3.83×10^{-3}	0.00
Maximum case based on the Fukushima monitoring data	3.39×10^{-3}	5.53×10^{-1}	5.19×10^{-2}	0.00
Geometric case based on the Fukushima monitoring data	7.46×10^{-4}	4.34×10^{-2}	1.25×10^{-2}	0.00

Table 3.

Calculation of the soil eroded per unit area in the 30 cases. The first digit of the three-digit numbers in the case name indicates R, the second indicates LS, and the third indicates C and P.

Case name	R	LS	C and P
111_s	USLE method	USLE method	Yamaguchi et al. (2013)
112_s	USLE method	USLE method	JWRC (2006)
113_s	USLE method	USLE method	Minimum case
114_s	USLE method	USLE method	Maximum case
115_s	USLE method	USLE method	Geometric mean case
121_s	USLE method	RUSLE method	Yamaguchi et al. (2013)
122_s	USLE method	RUSLE method	JWRC (2006)
123_s	USLE method	RUSLE method	Minimum case
124_s	USLE method	RUSLE method	Maximum case
125_s	USLE method	RUSLE method	Geometric mean case
131_s	USLE method	Stream power method	Yamaguchi et al. (2013)
132_s	USLE method	Stream power method	JWRC (2006)
133_s	USLE method	Stream power method	Minimum case
134_s	USLE method	Stream power method	Maximum case
135_s	USLE method	Stream power method	Geometric mean case
211_s	RUSLE method	USLE method	Yamaguchi et al. (2013)
212_s	RUSLE method	USLE method	JWRC (2006)
213_s	RUSLE method	USLE method	Minimum case
214_s	RUSLE method	USLE method	Maximum case
215_s	RUSLE method	USLE method	Geometric mean case
221_s	RUSLE method	RUSLE method	Yamaguchi et al. (2013)
222_s	RUSLE method	RUSLE method	JWRC (2006)
223_s	RUSLE method	RUSLE method	Minimum case
224_s	RUSLE method	RUSLE method	Maximum case
225_s	RUSLE method	RUSLE method	Geometric mean case
231_s	RUSLE method	Stream power method	Yamaguchi et al. (2013)
232_s	RUSLE method	Stream power method	JWRC (2006)
233_s	RUSLE method	Stream power method	Minimum case
234_s	RUSLE method	Stream power method	Maximum case
235_s	RUSLE method	Stream power method	Geometric mean case

Table 4.

Statistical indices of the discharge during the calculation period at each observatory.

Observatory	Observed (m^3 s^{-1})	Calculted (m^3 s^{-1})	MBE (m^3 s^{-1})	RMSE (m^3 s^{-1})	NSE (-)
Kosakuda	22.3	31.3	9.0	18.3	0.82
Miyota	37.3	45.0	7.7	26.3	0.83
Akutsu	52.9	61.2	8.3	36.3	0.86
Motomiya	63.9	73.9	10.0	44.3	0.81
Nihonmatsu	66.2	80.1	14.0	52.0	0.81
Kuroiwa	79.7	98.2	18.5	59.5	0.79
Fukushima	92.8	103.5	10.7	64.5	0.80
Fushiguro	108.4	121.2	12.9	76.5	0.81
Yahata	118.1	132.1	14.0	85.1	0.81

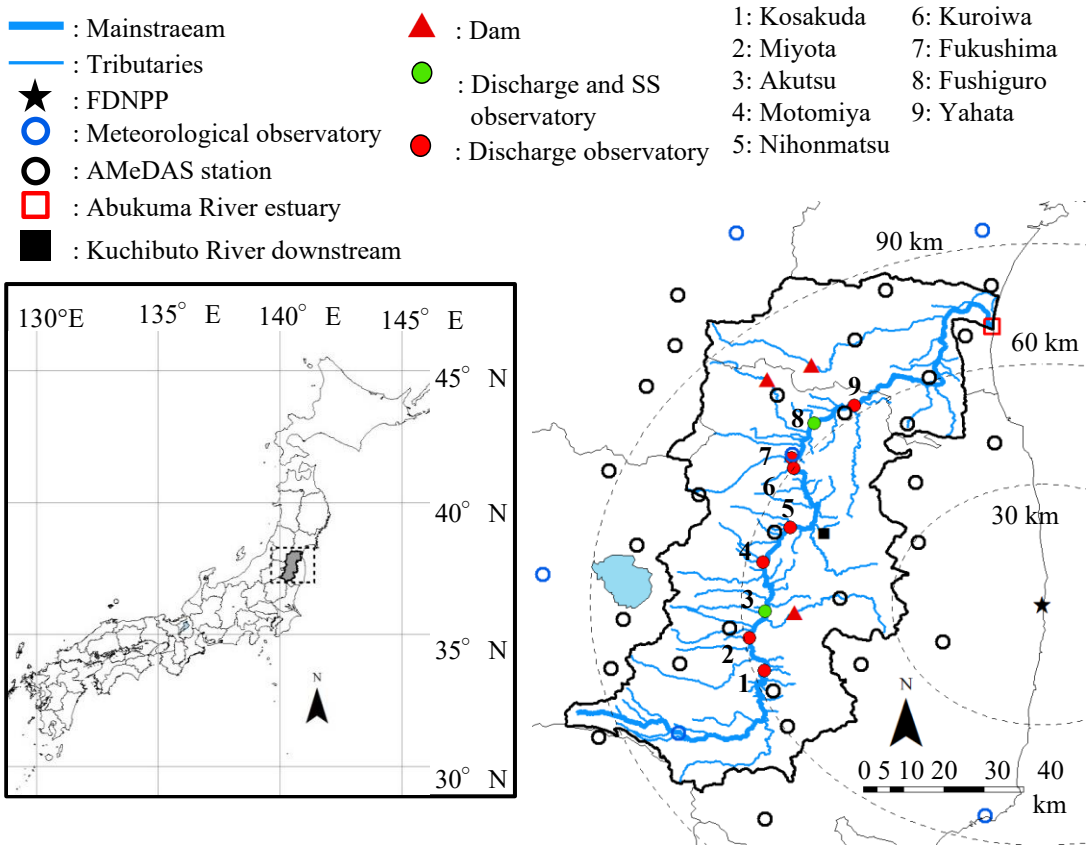

Fig. 1. Outline of the computational domain.

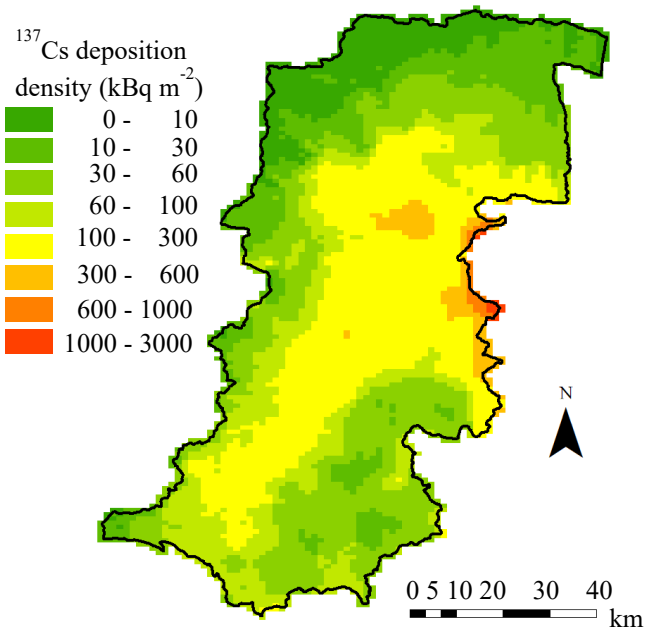

Fig. 2. Deposition density of ^{137}Cs measured by the airborne survey in May 2011 (MEXT et al., 2011b).

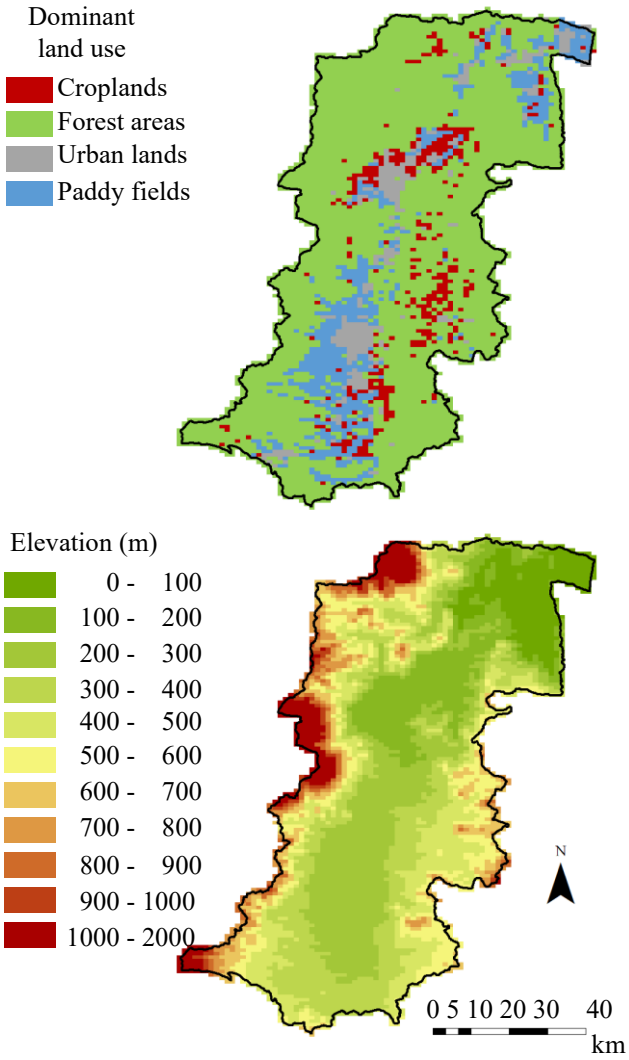

Fig. 3. Dominant land use and elevation in the computational domain (MLIT, 2011a). Dominant land were created by processing 1-km resolution land use data.

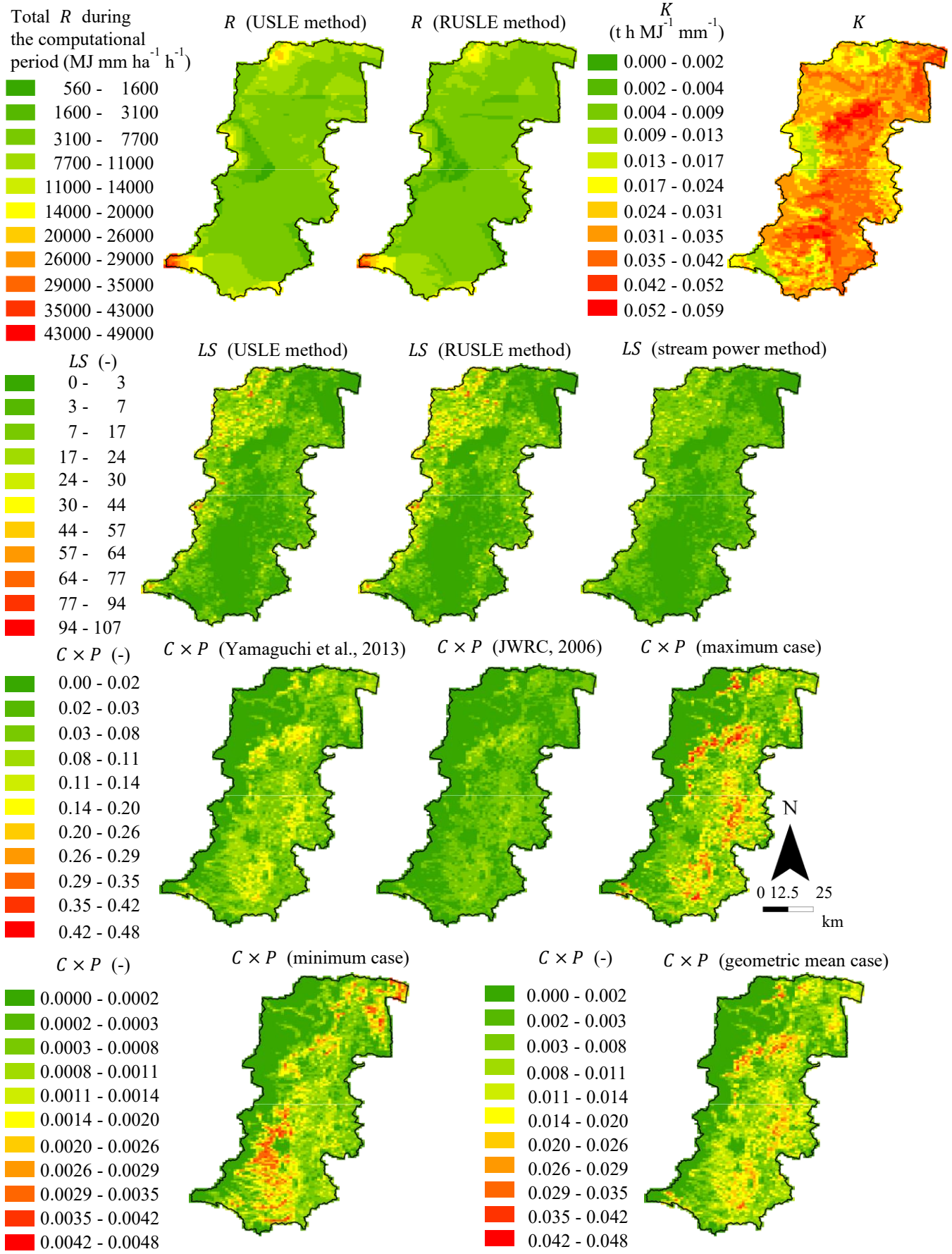

Fig. 4. The distribution of the USLE factors in the computational domain.

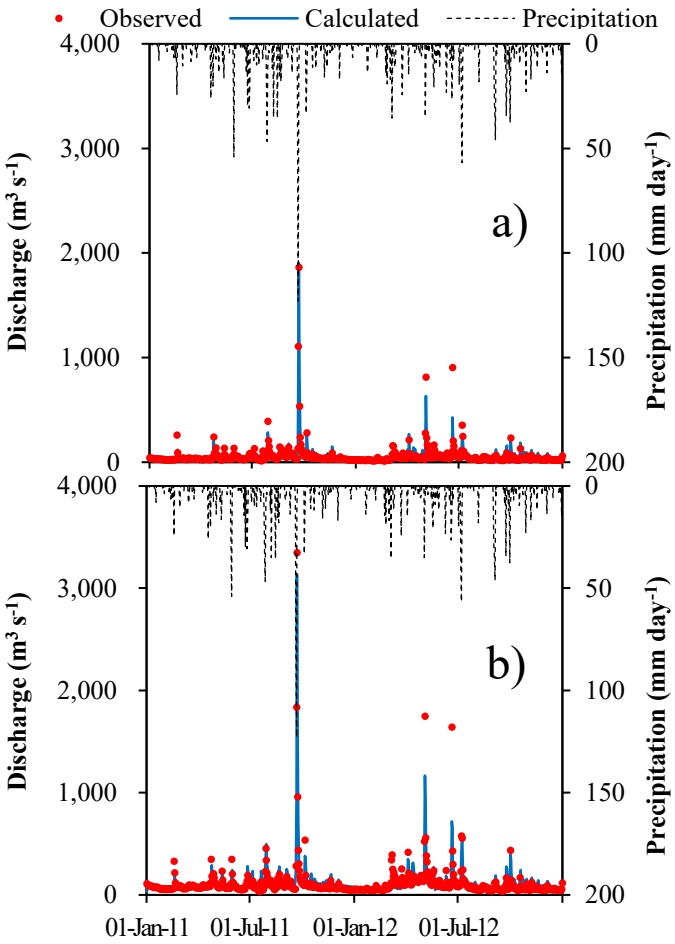

Fig. 5. Observed and calculated daily river flows at the a) Akutsu and b) Fushiguro observatories.

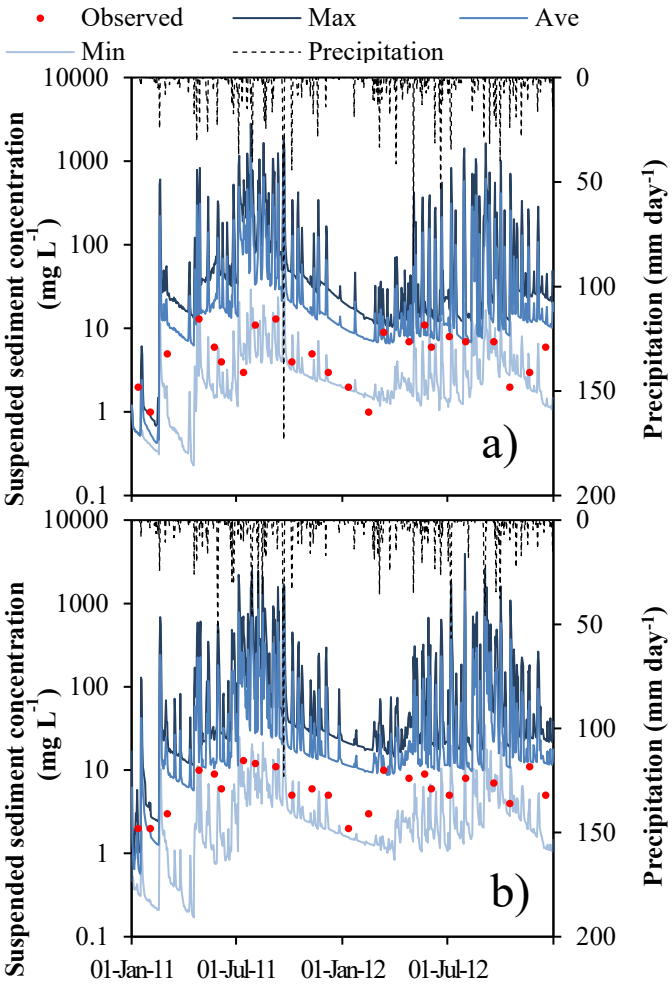

Fig. 6. Observed and calculated daily suspended sediment concentrations at the a) Akutsu and b) Fushiguro observatories. Max, Ave and Min in legend show maximum, average and minimum concentration in 30 simulation cases, respectively.

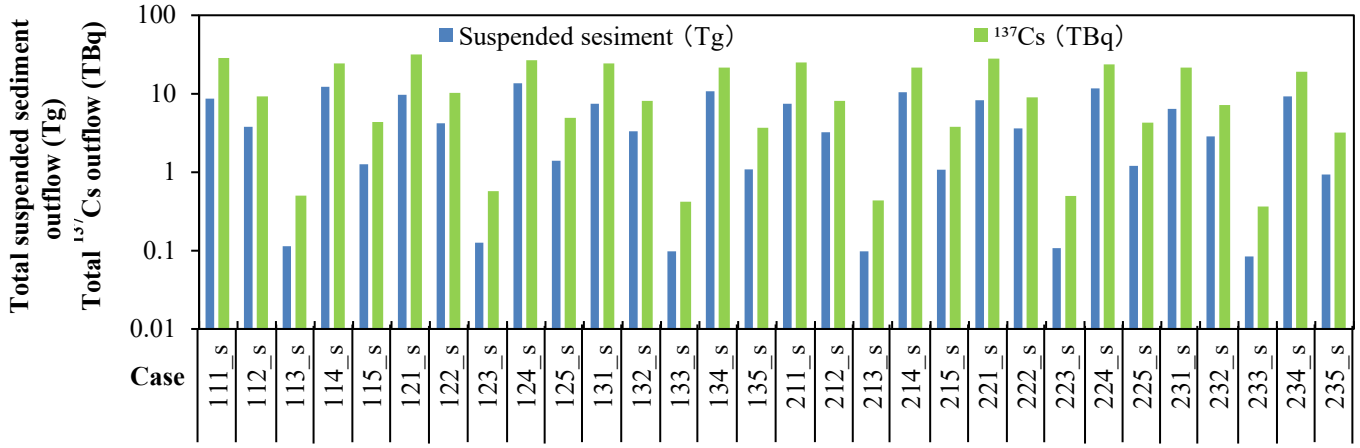

Fig. 7. The total suspended sediment and ^{137}Cs outflows during the computational period in the Abukuma River Basin in 30 simulation cases.

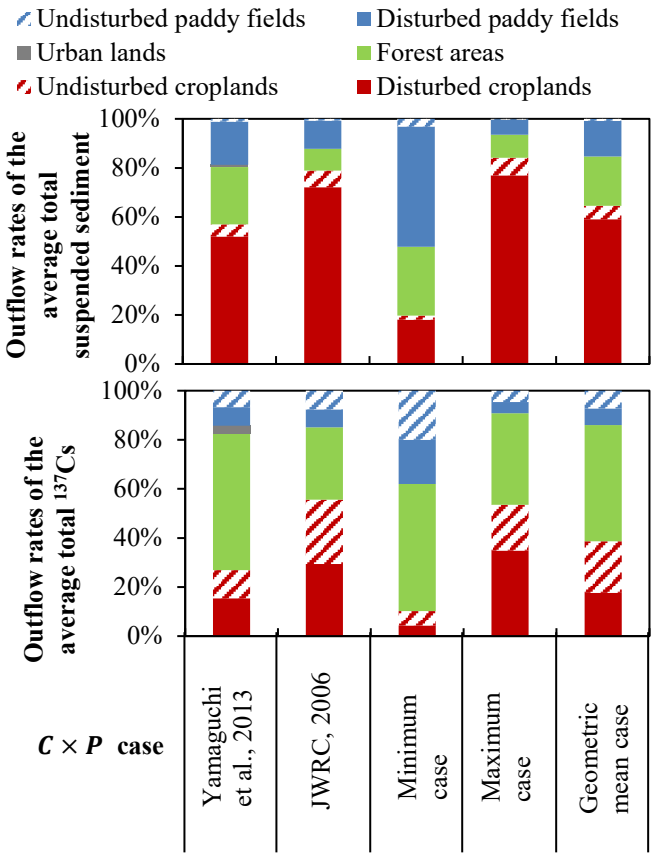

Fig. 8. The outflow rates according to land use of the average total suspended sediment and ^{137}Cs during the computational period in simulation cases using the same $C \times P$.

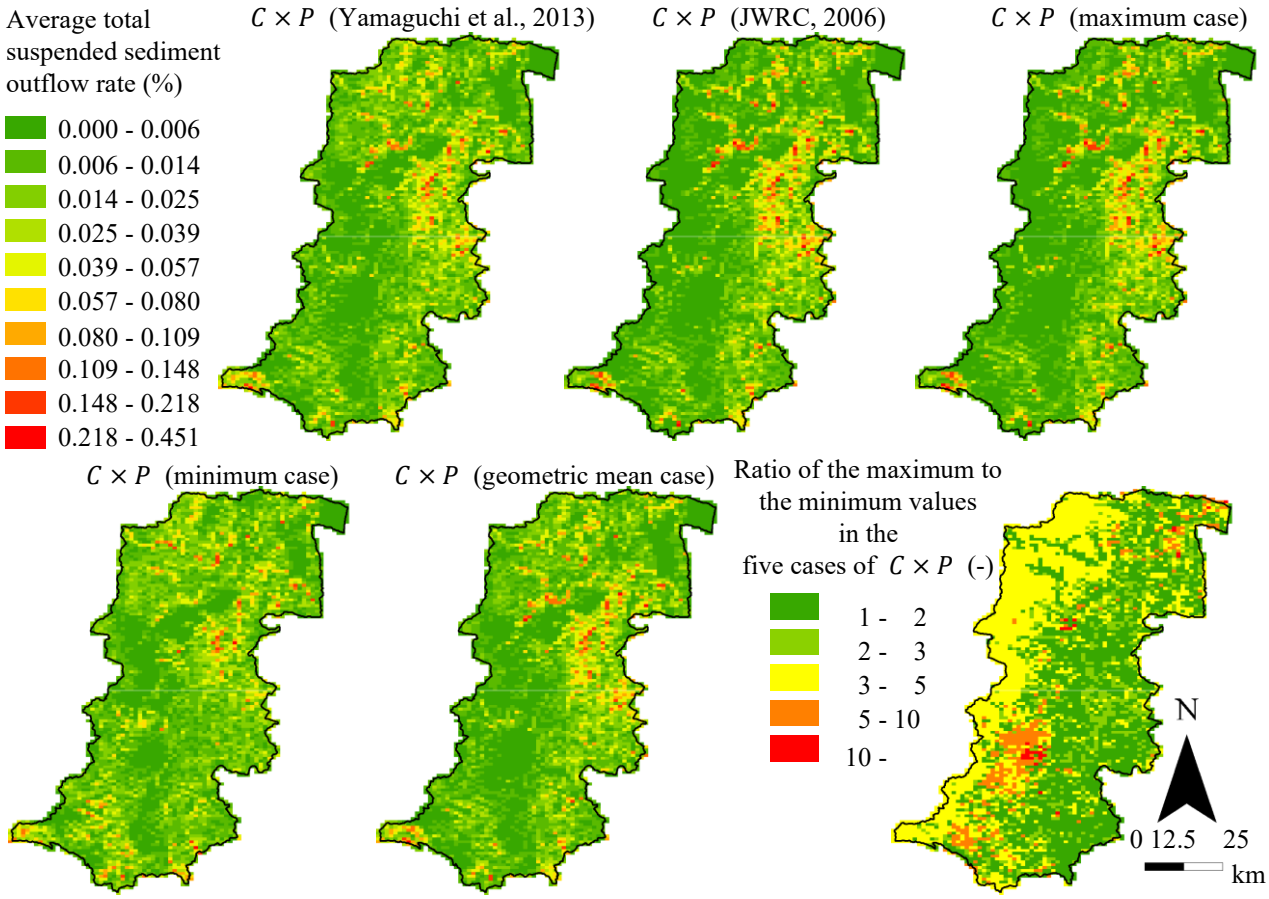

Fig. 9. Spatial distribution of the average total suspended sediment outflow rate during the computational period in simulation cases using the same $C \times P$. The panel on the bottom right corner shows ratio of the maximum to the minimum values in the five cases of $C \times P$.

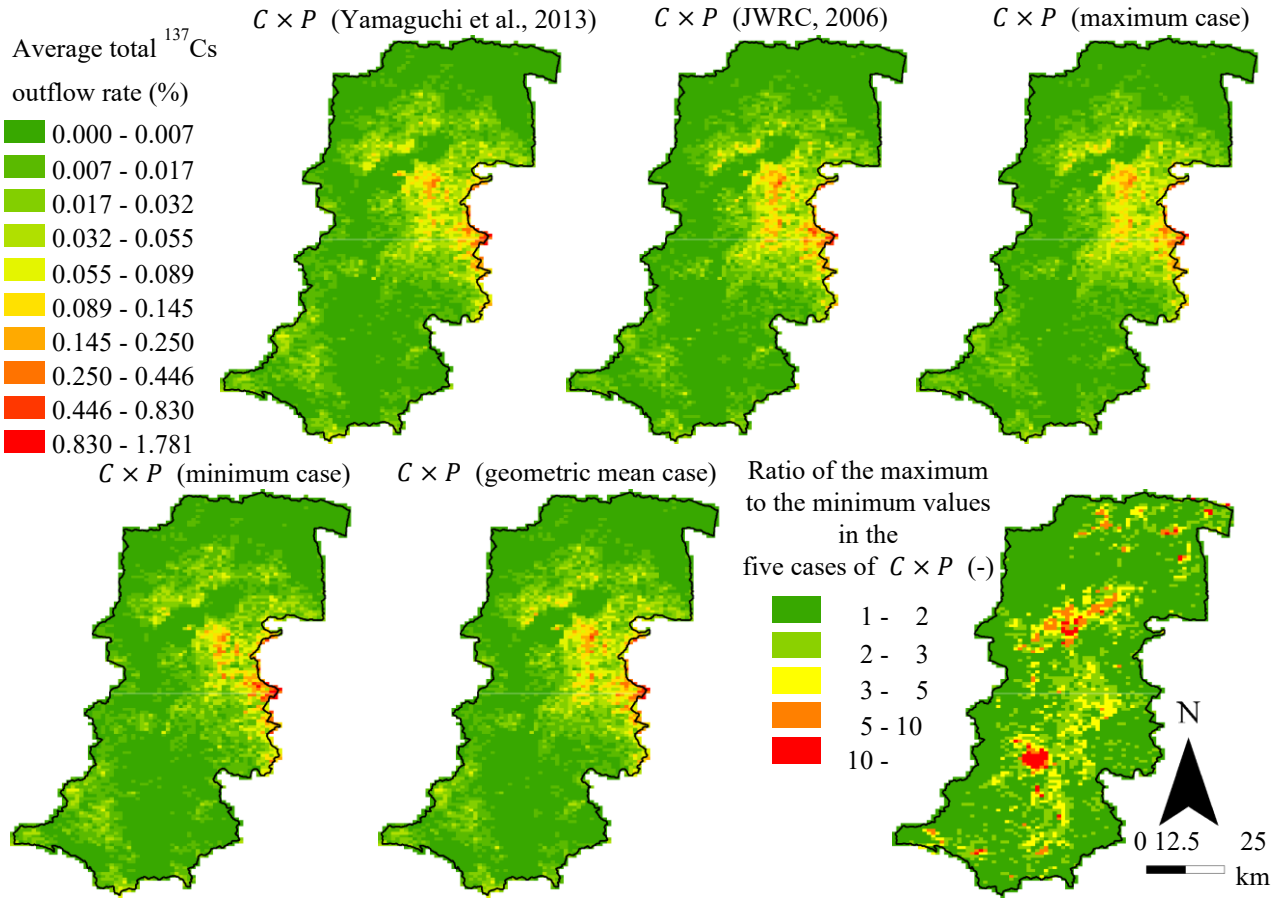

Fig. 10. Spatial distribution of the average total ^{137}Cs outflow rate during the computational period in simulation cases using the same $C \times P$. The panel on the bottom right corner row shows ratio of the maximum to the minimum values in the five cases of $C \times P$.

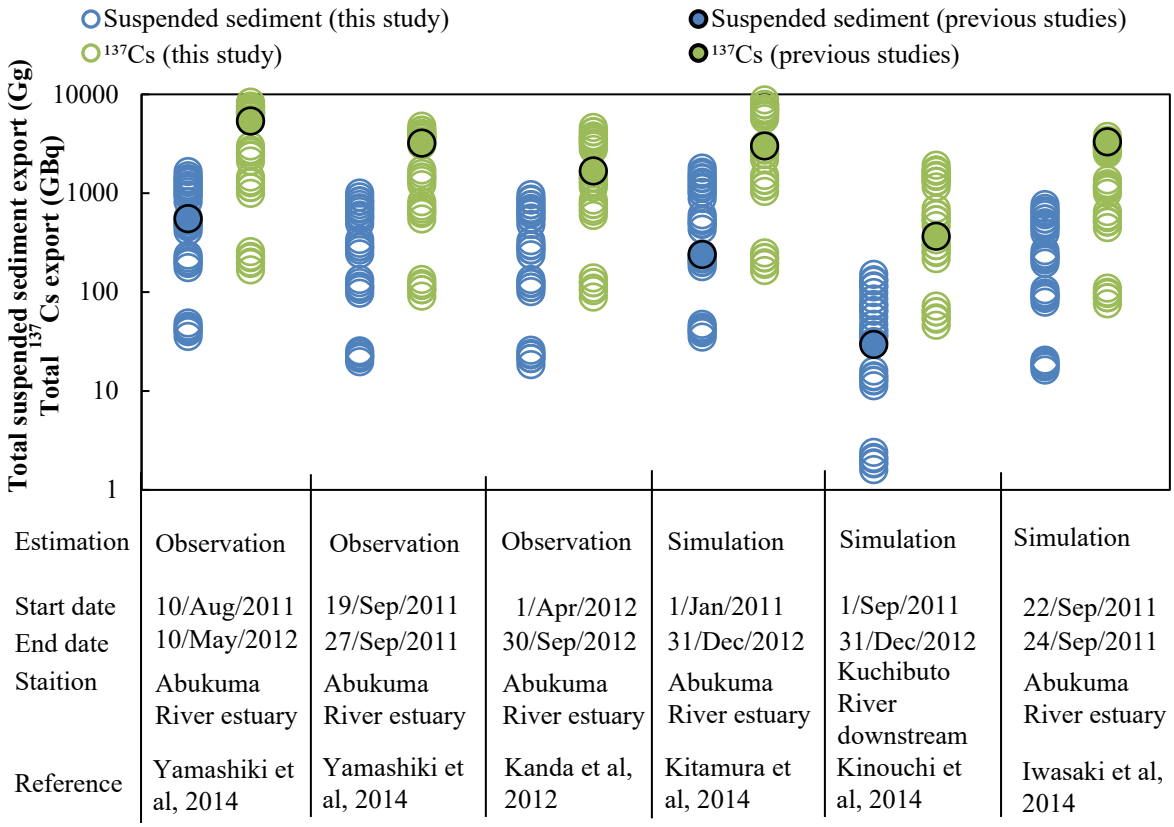

Fig. 11. Comparison of the 30 each calculated total exports of suspended sediment and ^{137}Cs to the values estimated previous studies. The estimated value based on the model of Kitamura et al. (2014) was compared to the annual average.